Quantitative HRTEM: A Novel Approach Towards Application Oriented Basic Research

Christian Kisielowski[a,b], Zuzanna Liliental-Weber[b] and Eicke R. Weber[a,b]

[a] *Department of Materials Science and Mineral Engineering*
University of California at Berkeley, Berkeley CA 94720

[b] *Lawrence Berkeley National Laboratory, Berkeley, CA 94720*

Received July 21, 1995

This paper reviews recent developments of microscopic methods that base on a quantitative analysis of electron micrographs to access subsurface systems at the atomic scale. It focuses on non-equilibrium diffusion processes that are observed in nanostructured MBE grown materials if a low growth temperature was used and on local deviations from a stoichiometric composition of materials. As examples we investigate GaAs/AlAs and Si/GeSi heterostructures and GaN single crystals. The purpose of the research is twofold. On the one hand it helps understanding physical processes at the atomic scale. On the other hand we can use the results to link basic physical knowledge with the performance of semiconductor devices made from nanostructured materials.

I. Introduction

Over the last decade a microscopic analysis of nanostructured materials had become both possible and necessary. Its feasibility is coupled to the development of analytic methods with atomic resolution and sensitivity such as Scanning Tunneling Microscopy (STM) and High Resolution Transmission Electron Microscopy (HRTEM). The methodological development is driven by the quest for a basic understanding of electronic, structural, optical and thermodynamic properties of solids at the atomic scale, by a semiconductor industry heading for deep sub-micron technology, including production of atomically engineered crystalline structures such as quantum wells, - wires and - dots and by the growth of new thin film materials such as III-V nitrides, to name a few reasons.

Nanostructured materials often contain large chemical gradients because they are grown at low temperatures to avoid intermixing of chemically or otherwise different components. Therefore, deviations from a thermodynamic equilibrium and from stoichiometry are almost unavoidable. They seem to be an intrinsic property of nanostructured materials. At this scientific and technological level there is growing need to extract structural and chemical information at a near-atomic scale to understand the underlying physical principles and processes.

In this paper we describe recently developed microscopic techniques that meet this needs and provide experimental data for the atomic scale structure and composition of nanostructured materials. The experiments to be described access subsurface regions and focus on non-equilibrium diffusion processes that seem to be typical for nanostructured materials, if grown at low temperatures, and on local stoichiometrical fluctuations. As examples we will describe transient diffusion processes in low-temperature (LT) grown LT- GaAs/AlAs - and Si/GexSix, heterostructures and deviations from stoichiometry in GaN bulk crystals. Relevance of the investigation for device processing will be documented.

II. Surface and subsurface region

Certainly STM has attracted a lot of attention in this field because its spatial resolution is better than 0.1 nm. This allows for mapping of individual atoms at surfaces and for investigations of single defects if located at surfaces or on the first few adjacent atomic layers[1].

Fig. 1 gives an example. There is no doubt that this method will continue to contribute with valuable results to the understanding of atomic-scale processes. In this paper, however, we focus on HRTEM and related techniques that do not exhibit the spectacular resolution of STM but offer different advantages. Consequently, we choose to look at STM and at HRTEM as complementary methods and not as competing ones.

HRTEM can be used to image individual atomic columns with a point resolution that recently reached 0.1 nm [2]. A very well established theory allows to approximate and to predict experimental results with high accuracy[3]. Standardized sample preparation techniques such as ion milling can be applied to prepare almost any material for a HRTEM investigation. In contrast to STM, HRTEM may be used to probe surfaces and subsurface regions because the electrons used for imaging transmit the samples. This is particularly of interest in cases where buried interfaces need to be studied with near atomic resolution. As an example for the ability of TEM to access the subsurface region we show in Fig. 2 a map of the Si/SiO_2 interface in a plan-view configuration. The thickness of the Si-crystal was reconstructed from the lattice image by QUANTITEM[4,5]. Since the crystal was covered by a 2 - 4 nm thick amorphous SiO_2 layer, the image displays the roughness of the crystalline material at the buried Si/SiO_2 interfaces in a similar way as Fig. 1 maps the atomic roughness of the cleaved GaAs [110] surface.

III. Quantitative high resolution transmission electron microscopy

Nowadays, many TEM and HRTEM investigations focus on a microscopic analysis of the structure and the composition of materials at the atomic scale. Approaches to access this information can be put together into two groups. One consists of building specially dedicated equipment such as energy filtered TEM[6], EELS[7] or Z-Contrast Microscopy[8]. The other one makes use of the fact that microscopes produce images. Taking advantage of the wide spread availability of electron microscopes and the increasing calculation speed of workstations and PC's it has become possible to analyze these images on a digital basis in order to extract quantitative information about the atomic scale structure, composition and thickness of the investigated materials. Out of the many approaches to quantify HRTEM[9–13] lattice images by image processing, we specifically report on results obtained by Chemical Imaging[14] and QUANTITEM[4,5].

Lattice images are electron interferrogramms. This is why any quantitative approach to interpret the pattern displayed by a lattice image requires theoretical guidance. The underlying physical process involved in lattice image formation is electron scattering at the crystal potential. Since this potential holds all information about the structure, composition and thickness of the investigated sample it is principally recoverable from any lattice image. However, experimental parameters, such as lens aberrations or the setting of the defocus modifies the pattern of lattice images. Thus, it is a methodological matter whether or not it is possible to extract the desired information from a lattice image. In this respect Chemical Imaging and QUANTITEM exhibit common features as well as distinct differences. Both methods use images digitized from the negative of a TEM plate. This offers the advantage that the image analysis is decoupled from taking them at an electron microscope. Pattern recognition is employed to quantify the information content of a lattice image as shown in Fig. 3. Differences of both methods are of physical origin. While Chemical Imaging is applicable to crystalline systems with chemical reflections and makes use of filter characteristics of the objective lens, QUANTITEM extracts functional dependencies from the lattice image itself and exploits knowledge of the extinction distances. Since knowledge of instrumental parameters such as the defocus setting is not required, QUANTITEM is principally applicable to any crystalline materials with coherent interfaces. Details of the procedures are described in references 5 and 14. In what follows we will concentrate on the atomic scale

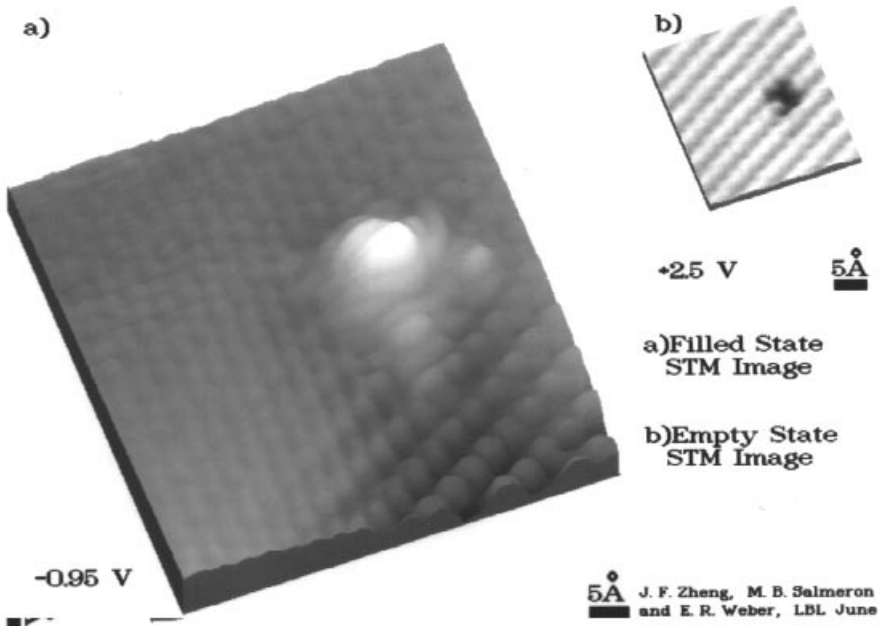

Figure 1. STM image of a cleaved GaAs [110] surface. The filled state image (a) reflects the positions of the As atoms, the empty state image those of the Ga atoms. The method allows for mapping of the atomic scale surface roughness and the detection of single defects. The single AsGa antisite defect can be seen to produce extra electron density in (a) and (b) proves the absence of a one Ga atom.

roughness of interfaces, on inter diffusion measurements on a 0.1 nm scale and on a local determination of absolute concentrations.

III.1 Diffusion in LT-GaAs/AlAs/GaAs heterostructures

Chemical Imaging was used first to investigate atomic scale diffusion processes[15]. Figs. 4 and 5 depict the potential of the method: The upper part of Fig. 4 displays a cross-section TEM image of the investigated heterostructures, the lower part a lattice image. Here the compositional change across the LT-GaAs/AlAs and the AlAs/GaAs interfaces is particularly of interest and it is encoded in the pattern of the lattice image. It changes from a fine to a coarse pattern as the interface is crossed from GaAs to AlAs. Chemical Imaging decodes this pattern change locally to produce a chemical map as shown in the upper part of Fig. 5. Average Al composition profiles, as depicted in Fig. 5, too, can be extracted by averaging the Al composition along atomic rows parallel to the interfaces. A quantitative value for the interfacial width can be obtained by fitting an error function erf (x/L) to the data, where x is the distance across the interface and $L = 2(Dt)^{1/2}$ is a diffusion length. A typical result of the fitting procedure is shown in Fig. 6. Thus, the diffusion length characterizes the abruptness of the chemical gradient. Its finite value indicates the presence of an atomiG scale roughness that is either caused by the growth procedure or by Al inter diffusion during growth and during post-growth annealing.

We investigated four samples with a layer spacing shown in Fig. 4. All growth and annealing steps were kept constant except the growth temperature of the LT-GaAs layers. It was varied between 170°C and 250°C. A 10 minutes annealing after growth was performed at 600°C to create a semi-insulating LT-GaAs layers. The annealing procedure is known to create As precipitates[16] that are visible in Fig. 4. The central GaAs layer was Si doped [$6^{*}10^{17}$ cm^{-3}]. Results on the atomic scale roughness measurements are shown in Fig. 7. Gate-drain breakdown voltages were measured by I(V) characterization of the heterostructures. They

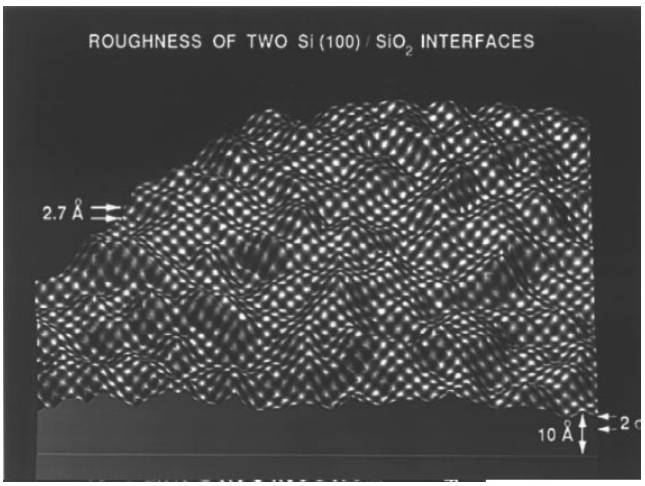

Figure 2. Atomic scale roughness mapping of buried Si/SiO_2 interfaces. Since QUANTITEM measures the thickness of finite atomic columns, the image is a superposition of two such interfaces. Note that the crystalline material is buried under a 2 - 4 nm thick amorphous overlayer. The experimental lattice image is displayed on top of the surface.

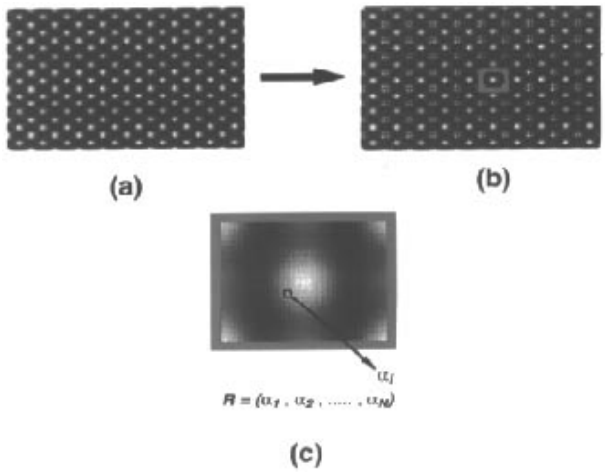

Figure 3. Formation of unit cells and image vectors in a pattern recognition procedure. (a) lattice image, (b) definition of unit cells by introduction of a periodical grid; (c) creation of image vectors that quantify the information content of one unit cell. The lateral resolution of the method is given by the size of the unit cell [0.3nm x 0.3nm in case of Si (100)]. A lattice image provides roughly 1000 image vectors. Their dimension is determined by the number of pixels in each unit cell.

are compared with Al inter diffusion data in Fig. 8. The results of Figs. 7 and 8 can be summarized as follows:

a) In the LT-GaAs layer closest to the surface, the Al inter diffusion increases monotonically with decreasing growth temperature of the LT-GaAs layers.
b) At all other interfaces the Al inter diffusion exhibits a maximum at a LT-GaAs growth temperature of 190°C.
c) The Al inter diffusion into the Si doped GaAs is slightly larger than into the adjacent LT- GaAs if the samples are grown between 190°C and 270°C. Growth at 170°C inverts this tendency.
d) The gate-drain breakdown voltages and the Al inter diffusion exhibit a similar maximum (Fig. 8) in particular at interfaces adjacent to the GaAs:Si layer.

We consider Al/Ga inter diffusion to be the main cause for the formation of rough interfaces and we interpret our results in terms of diffusion processes. Al/Ga inter diffusion is mediated by Ga vacancies on the group III sublattice of the zincblende structure[15]. Therefore, an increase of the Al diffusion length with decreasing growth temperature of the LT-GaAs layers requires an increasing supersaturaturation of the VGa concentration. Consequently, the observed effects must be attributed to the presence of non-equilibrium point de-

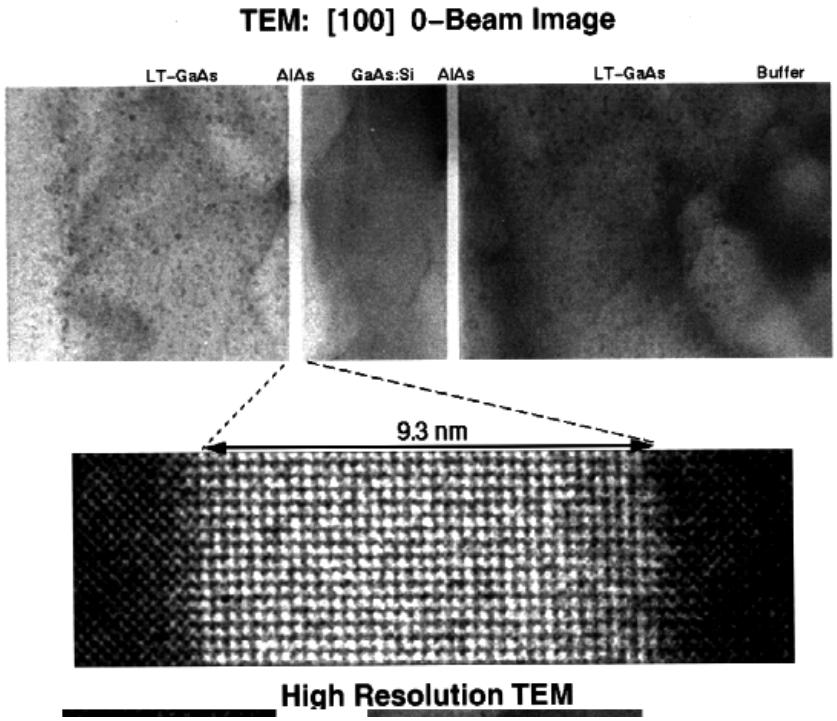

Figure 4. Upper part: Cross-section TEM-image of the investigated structure. The location of the different layers is indicated. The LT-GaAs layers are grown between 170°C and 250°C and are sources of supersaturated vacancies. The central GaAs layer is Si doped; [Si] = 6 10^{17}cm^{-3}. The AlAs and GaAs:Si layers were grown at 600°C. As a consequence of the growth procedure, the LT-GaAs layer adjacent to the buffer is annealed during growth and during the post-growth annealing step. Arsenic precipitation is confined to the LT-GaAs layers and caused by annealing. Lower part: Lattice image of the first AlAs quantum well. The transition from a coarse to a fine pattern in the image is caused by a changing Al concentration.

fects frozen-in during the growth procedure. This interpretation is supported by an earlier investigation on the formation of As precipitates in LT-GaAs[16] that indicated the presence of Ga vacancies which contribute to the Oswald ripening of the As precipitates. In Fig. 9 we depict the exact heat treatment during sample growth and the expected VGa concentration profiles in case of out-diffusion of supersaturated vacancies. In this picture we neglected contributions from in-diffusion of vacancies generated at surfaces as observed in reference[15], because their contribution to the Al inter diffusion in our samples can quantitatively be determined to be small. Certainly, any annealing after growth will redistribute the supersaturated Ga vacancy concentration. Details of the results are published elsewhere[17]. Here, we address three issues.

First, the experiment proves that with decreasing LT-GaAs growth temperature an increasing supersaturation of point defects can be achieved. In our experiments the vacancy supersaturation factor varies between 10 and 100 if the LT-GaAs growth temperature is reduced from 250°C to 170°C.

Second, we make use of the fact that the supersaturation can be confined to some part of the heterostructure. This allows to study the impact of diffusion on electrical properties of devices. In this particular case, the gate breakdown voltage of a MESFET made from this structure is either determined by the trap filled limit voltage[18] of the LT- GaAs layer closest to the surface or by avalanche breakdown in the GaAs:Si channel. Recently, pairing of vacancies with Si atoms in LT-GaAs has been observed experimentally[19]. Enhanced diffusion of SiGa-VGa pair has been predicted theoretically[20]. However, it was not possible to study the impact of Ga vacancy diffusion on the SiGa-VGa pair formation during device processing. Thus, our experiments suggest for the first time that Ga vacancy diffusion and pairing effects contribute to the avalanche breakdown in the channel. We study basic physical pro-

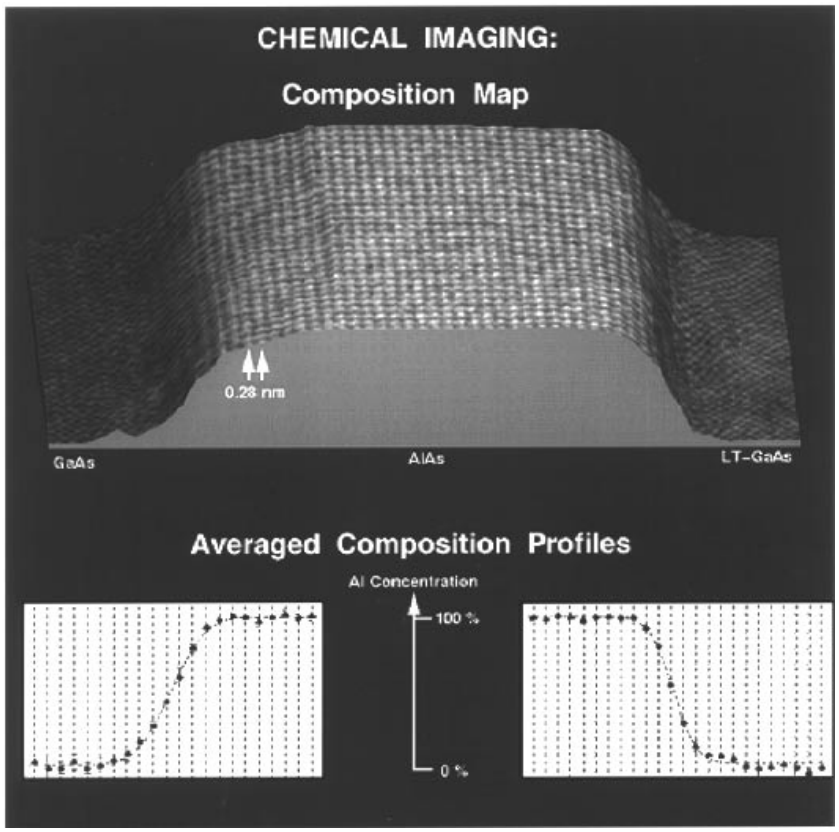

Figure 5. Upper part: Chemical map obtained from a quantitative analysis of the lattice image shown in Fig. 4 by Chemical Imaging. Lower part: Averaging of atomic columns along the quantum well gives the displayed composition profile across the interfaces that are of different width. The measurement is relative and requires knowledge of the composition in two areas at some distance from the interface (100% GaAs and 100% AlAs in this case).

cesses and relate them to the performance of devices.

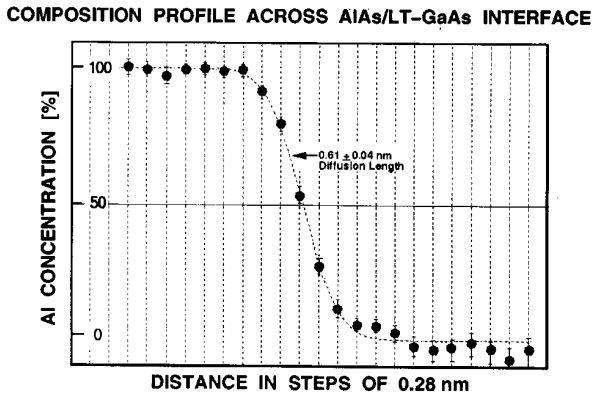

Figure 6. Determination of the Al/Ga inter diffusion length $L = 2\ (D\ t)^{1/2}$ by fitting an erf (x/L) to the data. The distance across the interface x is measured in steps given by the size of the unit cells.

Third, the presence of free and internal surfaces and the finite migration distance of vacancies influence and limit the diffusion process. The formation of VGa concentration gradients is, therefore, expected. In the sample with the LT-GaAs layers grown at 190°C the sample surface seems to act as a sink for VGa which is why less Al/Ga inter diffusion occurs at comparable interfaces that are closer to the samples surface (Fig. 7). In the sample grown at 170°C, however, migration of vacancies from the LT-GaAs into the GaAs:Si seems to be a limiting process that causes a larger intermixing at the AlAs/LT-GaAs interfaces compared with the AlAs/GaA:Si interfaces and, thereby, causes an inversion of the trends observed at higher LT-GaAs growth temperatures (Fig. 7). We will show in the next paragraph that the formation of vacancy gradients in surface proximity can be observed in other materials systems, too, if grown at low temperature.

In summary we show for the first time that there is a correlation of the Al/Ga inter diffusion and the gate breakdown voltage in LT-GaAs/AlAs/GaAs:Si based devices. We attribute this effect to the diffusion of supersaturated Ga vacancies and their interaction with Si

donor atoms. We find evidence for the formation of vacancy gradients in surface proximity and a limitation of the diffusion process by the vacancy migration distance if the LT-Layer is grown at 170°C.

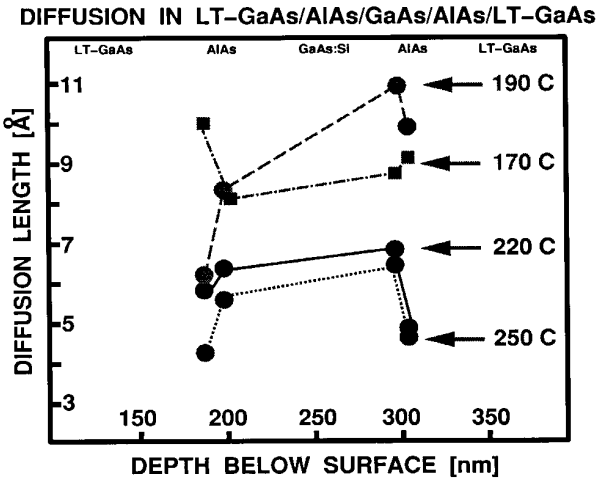

Figure 7. Measured Al/Ga inter diffusion length at the interfaces of the investigated structure. Their location is measured from the surface of the crystal. The growth temperature of the LT-GaAs layers is indicated. For simplicity no experimental errors are plotted. They are typically of 0.1nm as shown in Fig. 8. Note the monotonic increase of the diffusion length at the first LT-GaAs/AlAs interface and the occurrence of a maximum at all other interfaces for a LT- GaAs growth temperature of 190°C.

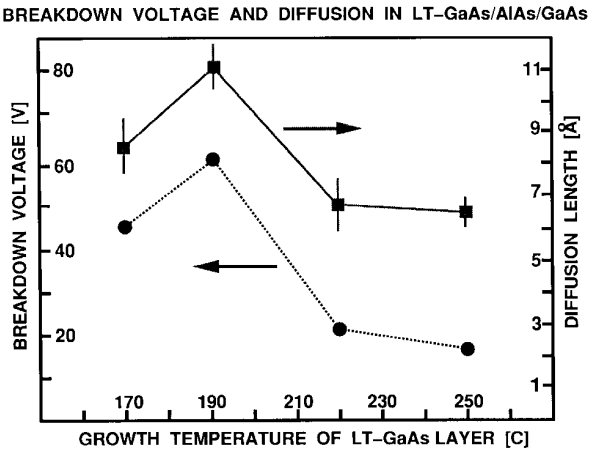

Figure 8. Dependence of the gate breakdown voltage on the growth temperature of the LT-GaAs. layer. The results are compared with the Al/Ga inter diffusion length measured at the second GaAs:Si/ AlAs interface. The graph shows the accuracy as to which the diffusion length has to be measured to observe this correlation.

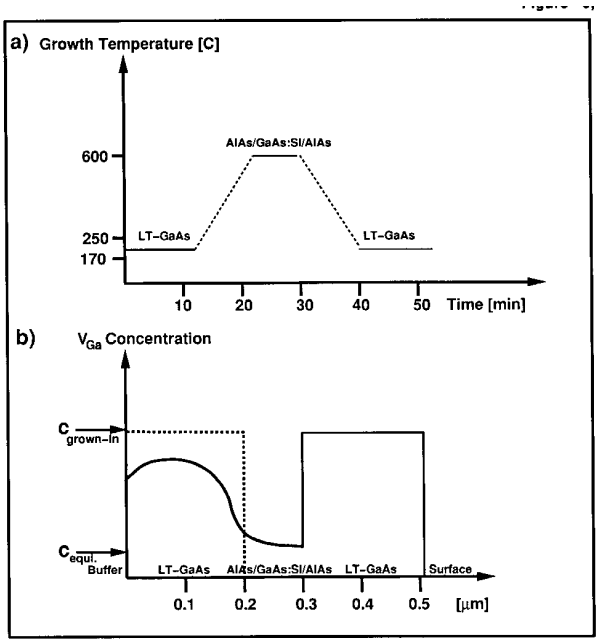

Figure 9. (a) variation of the growth temperature during sample growth.(b) Model of the assumed Ga vacancy concentration in the structure. In the LT-GaAs closest to the buffer the initial vacancy supersaturation is redistributed during sample growth. A post-growth annealing step changes the vacancy distribution in all layers. Note that we expect the lowest vacancy concentration in the GaAs:Si layer. Yet the Al/Ga inter diffusion is the largest at AlAs/GaAs:Si interfaces if the LT-layers are grown above 170°C (Fig. 7). This requires a larger mobility of the vacancies in GaAs:Si that we attribute to SiGa-VGa pairing effects.

III.2 Diffusion in Si/Ge025 Sio 7s /Si heterostructures

Application of Chemical Imaging is restricted to materials with chemical reflections such as $Al_xGa_{1-x}As$[15] or $In_xAl_{1-x}As$[21,22]. The recent introduction of QUANTITEM allows to apply quantitative HRTEM to general crystalline materials systems. QUANTITEM has been used to investigate the roughness of the buried Si/SiO_2 interface (Fig. 2) and the Ge inter diffusion in the MBE-grown $Si/Ge_{0.25}Si_{0.75}/Si$ heterostructure that is shown in Fig. 10. This structure was grown at low temperature (500°C) to study transient diffusion phenomena that we expect to occur in surface proximity. Fig. 11 depicts a Ge composition map extracted from a lattice image by QUANTITEM. Averaging of the Ge concentration along atomic rows parallel to the quantum wells allows for an extraction of averaged composi-

tion profiles as shown in Fig. 12. Two conclusions can be drawn from the figure: First, the interfaces are not atomically abrupt but extend over roughly 1nm. Second, the Ge distribution is symmetric with respect to the growth direction, proving that in this case growth of Si on $Ge_{0.25}Si_{0.75}$ or vice versa does not result in a different interfacial width. However, the existence of a diffusion tail formed by Ge concentrations smaller than 1% cannot be excluded for sensitivity reasons.

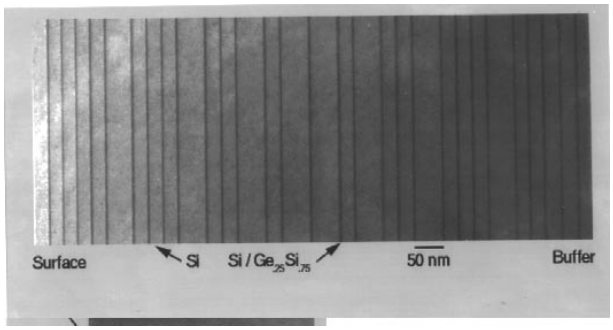

Figure 10. Cross-section TEM image of the $Si/Ge_{0.25}Si_{0.75}$ heterostructure used to investigate the influence of a free surface on the out-diffusion of supersaturated vacancies.

Next, we concentrate on the width of the quantum wells after growth and after annealing of this structure at 800°C in an argon atmosphere for 5h (Fig. 13). It can be seen that a nominal layer thickness of 5nm could be reproduced within ~0.5 nm and that there is a tendency that layers closer to the buffer are broader compared with those close to the surface. This indicates some Ge/Si inter diffusion during growth of the sample. After annealing the quantum well width increases and the amount of broadening depends on its position below the sample surface. It is expected that Ge diffusion in silicon is mediated by the Si vacancy at 800°C[23]. Therefore, a dilution of supersaturated vacancies in surface proximity and probably also towards the buffer layer is likely to cause the depth dependence of the quantum well width. A quantitative description of the out-diffusion process that includes strain relaxation effects will be given elsewhere[24]. Here, it is particularly of interest that both, the LT-GaAs layers as well as the Ge/Si heterostructure is a source of supersaturated vacancies which become mobile during annealing at temperatures higher than the growth temperature.

Thus, we see that a supersaturation of point defects during MBE growth is a common phenomena if the growth temperature of the layers is low. Any processing of such material might reveal unusual effects that can be related to non-equilibrium diffusion phenomena by use of heterostructures as marker layers for the point defect diffusion and by application of quantitative HREM.

IV. Convergent beam electron diffraction (CBED)

Quantitative HRTEM can be used to map the composition and the materials thickness at the atomic scale. Presently, it is desirable to implement this principle for more complex systems such as hexagonal structures. This is a methodological matter. Principally, however, QUANTITEM is no spectroscopic method. Knowledge of the samples composition in two areas in the field of view is required. In case of quantum well structures this information can easily be provided, e.g. RBS may provide sheet concentrations in a quantum well and quantitative HRTEM its width. This procedure was used for calibration of the Ge concentration in our Ge/Si heterostructure. However, there are other situations where the materials composition may vary locally in an unpredictable manner. For example, in new materials such as bulk GaN compositional fluctuations are expected because bulk GaN is grown under exotic conditions (Ga rich, growth temperature: ~1500°C, hydrostatic nitrogen pressure: ~1.5 GPa). Here, a local determination of the absolute concentration is desirable but cannot be provided by quantitative HRTEM at this point.

In order to contribute to a solution of this problem we explored the chemical sensitivity of CBED. Capabilities of this method has recently been reviewed[25]. Quantitative image analysis procedures for CBED patterns are currently being developed[26]. As to our

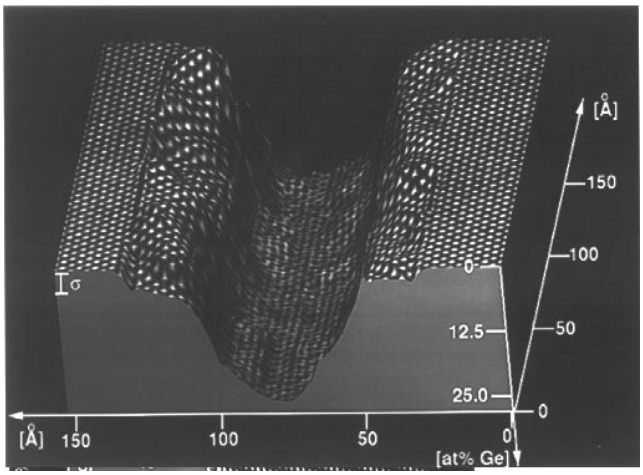

Figure 11. Ge concentration map obtained by QUANTITEM from a lattice image of one quantum well of the heterostructure shown in Fig. 10. The experimental lattice image is displayed on top of the surface.

knowledge, however, no attempted has yet been made to use CBED patterns for the determination of the absolute composition, particularly of bulk GaN. Fig. 14 shows that the experimental CBED pattern recorded along a [1-100] zone axis of bulk GaN can be reproduced by image simu!ation. The Fig. also depicts that an incorporation of the six native point defects into the simulation, that change the crystal stoichiometry, causes significant deviations from the experimental pattern. Particularly, the presence of Ga interstitials (Ga_i) and Ga_N antisite defects introduces distinct and strong deviations from the experimental pattern. In fact, we measured in different areas of bulk GaN single crystal different CBED patterns experimentally[27]. They are shown in Fig. 15 and compared with simulations. It can be seen that we can simulate the thickness dependence of the CBED pattern. Also, we can match the two different experimental images, taken at the same crystal thickness but in different extended defect free areas, with one certain set of simulation parameters by the introduction of GaN antisite defects. In this case, thickness and composition can hardly be confused and the image matching could not be achieved by the introduction of another native point defect into the simulation. We also show that the incorporation of nitrogen vacancies changes the CBED patterns only slightly. Thus, the chemical sensitivity of CBED strongly depends on the scattering power of the involved defects that changes the extinction distance. It is rather unexpected to detect such a large deviation from the stoichiometric composition of bulk GaN.

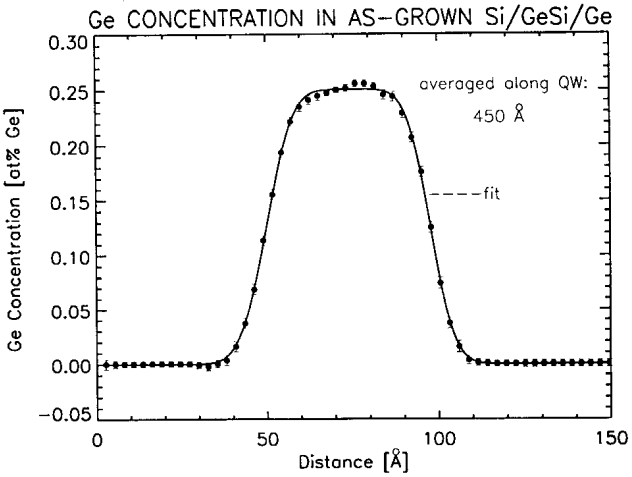

Figure 12. Extraction of a Ge concentration profile by averaging the Ge concentration along atomic columns parallel to the well. Fitting of two erf (x/L) allows for a quantification of the interfacial - and the well width. Note that the averaging reduces the error bars to the size of the dots.

At this point we stress that image matching by visual inspection is commonly used in HRTEM and CBED. However, this is not a quantitative method. It is for this and for experimental reasons that we cannot yet give absolute numbers for defect concentrations. Also, the introduction of defect complexes involving GaN antisite defects will cause similar CBED patterns.

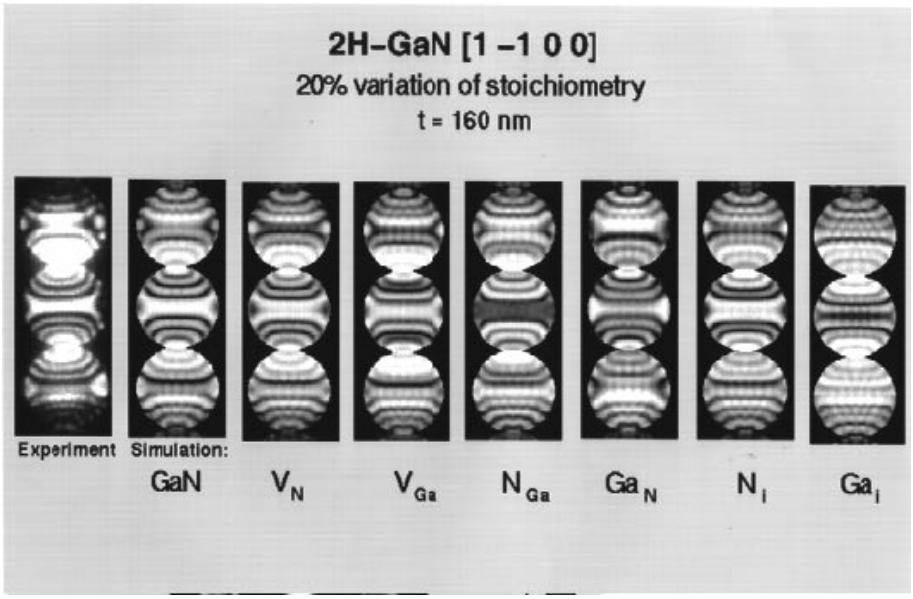

Figure 14. Comparison of an experimental CBED image taken along a [1-100] zone axis with an image simulation. From visual inspection it can be seen that detailed agreement can be achieved. It is also shown that an introduction of native point defects into the image simulation causes significant changes of the CBED pattern. These patterns hold the information about the local (∼2 nm lateral resolution) stoichiometry of the GaN crystal.

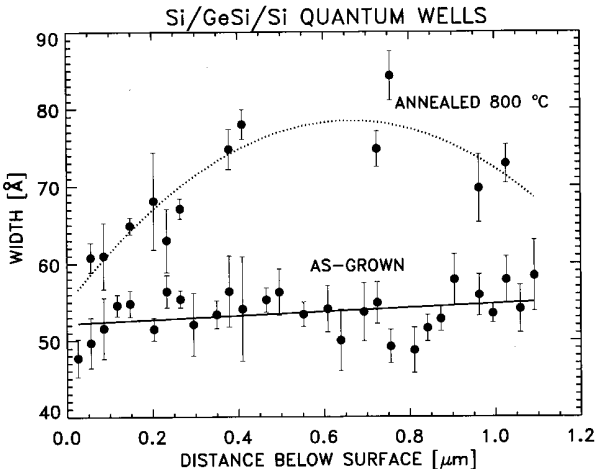

Figure 13. Width of the Ge quantum wells after growth and after annealing at 800°C in an argon atmosphere. The small Si/Ge inter diffusion in surface proximity and probably also in the proximity of the buffer indicates that the surface and the bulk grown silicon are sinks for out- diffusing vacancies.

Thus, we conclude that CBED is potentially suitable to provide local information of the absolute chemical composition of crystalline materials. In case of bulk GaN, we give evidence for the presence of a large (range of %) Ga supersaturation that varies locally. The supersaturated Ga atoms seem to occupy nitrogen sites forming GaN antisite defects or defect complexes that contain GaN antisite defects. It is striking that theoretical calculations[28] cannot explain the presence of the large (102° cm^3) native defect concentration in bulk GaN. Instead, the calculations predict the formation of N vacancies and Ga interstitials with concentrations up to 10^{17} cm^{-3}. Provided that the theoretical result holds qualitatively, our experiment suggests that a reaction $Ga_i + V_N \rightarrow Ga_N$ is energetically favorable. We speculate that the large hydrostatic pressure during growth and cooling of the bulk GaN crystals strongly influences the formation of native point defects.

V. Conclusions

In this paper we review some of the recent achievements of quantitative HRTEM. Up to now quantitative HRTEM is one of the rare tools that accesses the subsurface region with near atomic resolution and sensitivity. Here, we concentrate on the investigation of non- equilibrium diffusion processes that occur during processing of MBE grown samples if the sample growth was performed at low temperatures. The increasing diffusion with decreasing LT-GaAs growth temperature in LT-GaAs/AlAs/GaAs:Si heterostructures documents a large deviations from the thermodynamic equilibrium. Vacancies are frozen-in during sample growth and supersaturation factors can reach 100 in LT-GaAs.

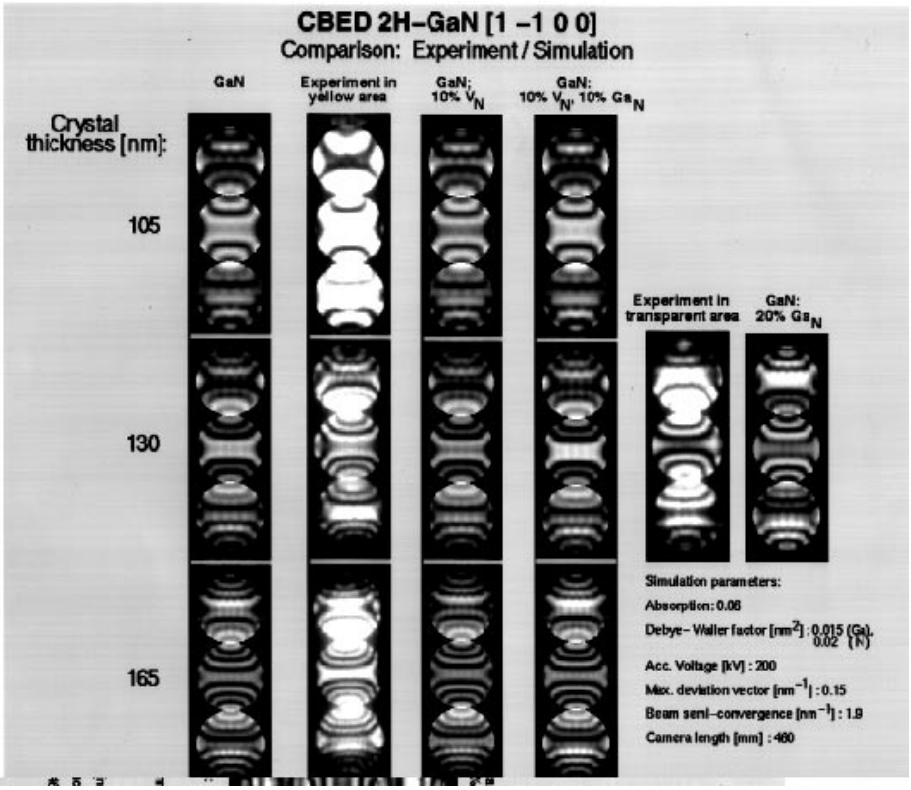

Figure 15. Bulk GaN crystals exhibit optically different yellow and transparent areas. Experimental CBED patterns taken from such areas are distinctly different as shown in the image. For the listed set of simulation parameters it is possible to simulate the thickness dependence of the CBED pattern as well as the compositional change but only if attributed to the presence GaN antisite defects. The simulation also shows that the presence of VN hardly can be detected as long as no quantitative image analysis is applied.

A transient diffusion process from supersaturated vacancy concentrations causes a depth dependence of the diffusion coefficient close to free or internal surfaces. In the LT-GaAs/AlAs/GaAs:Si heterostructures we exploit the initial spatial separation of the vacancies from the Si donors to show that vacancy diffusion affects the Si concentration by redistribution and/or donor-vacancy pairing. Therefore, the diffusion process modifies the breakdown voltage of rectifying devices that contain LT-GaAs layers.

We provided a glimpse on future areas that might help to develop this new field of activities. Apart from implementing QUANTITEM for more complex structures, we find that CBED is well suited to complete quantitative HRTEM because of its ability to measure absolute compositions locally. We document this ability of CBED by proving evidence for a local deviation from the stoichiometric composition of bulk GaN.

It is the purpose of our investigations to extend our knowledge to a point that allows a quantitative extraction of the formation - and migration enthalpies or of the supersaturation of native point defects, to name a few physical quantities. However, our approach not only aims for a better understanding of physical processes on an atomic scale. It also helps to link this fundamental knowledge with the performances of devices made from nanostructured materials.

Acknowledgments

The research was supported by AFOSR-ISSA-90-0009. The use of the ARM microscope in the National Center for Electron Microscopy in Lawrence Berkeley National Laboratory supported by the Director, Office of Energy Research, Office of Basic Energy Sciences, Materials Science Division of the U.S. Department of Energy under contract no. DE-AC03- 76SF00098 is greatly appreciated. Experiments on Ge/Si heterostructures were performed in the Microphysics De-

partment at AT&T Bell Laboratories with kind support of A. Ourmazd. The authors thank W. Swider for careful and successful TEM sample preparation.

References

1. J. F. Zheng, J. D. Walker, M. B. Salermon, E. R. Weber, Phys. Rev. Lett. **73**, 368 (1994).
2. A. Orchowski, W. D. Rau, H. Lichte, Phys. Rev.Lett. **74**, 339 (1995).
3. see e.g. J. C. H. Spence, *Experimental High Resolution Electron Microscopy*, (Clarendon, Oxford, 1981).
4. P. Schwander, C. Kisielowski, M. Seibt, F. H. Baumann, Y. Kim, A. Ourmazd, Phys. Rev. Len. **71**, 4150 (1993).
5. C. Kisielowski, P. Schwander, F. H. Baumann, M. Seibt, Y. Kim, A. Ourmazd, Ultramicroscopy **58**, 131 (1995).
6. S. Kujawa, D. Krahl, H.Niedrig, E. Zeiler, Optik **86**, 39 (1990).
7. see e.g. C. C. Ahn, M. Dicko, EELS in *Materials Science, The Metals Society*, London, 1992.
8. S. J. Pennycook, D. E. Jesson, Ultramicroscopy **37**, 14 (1991).
9. K. H. Downing, H. Meisheng, H.-R. Weng, M.A. O'Keefe, Nature **348**, 525 (1990).
10. D. Van Dyck, M. Op de Beeck, Optik **93**, 103 (1993).
11. A. Thust, M. Lentzen, K. Urban, Ultramicroskopy **53**, 101 (1994).
12. G. Moebius, M. Ruehle, Ultramicroscopy **56**, 54 (1994).
13. A. Bourret, J.-L. Rouviere, J.-M. Penisson, Acta Crys. A**44**, 838 (1988).
14. A. Ourmazd, D.W. Taylor, M. Bode, Y. Kim, Science **246**, 1571 (1989).
15. J.-L. Rouviere, Y. Kim, J. Cunningham, J. A. Rentschler, A. Bourret, A. Ourmazed, Phys. Rev. Letters **68**, 1992 (2798).
16. Z. Liliental-Weber, X. W. Lin, J. Washburn, Appl. Phys. Lett. **66**, 2086 (1995).
17. C. Kisielowski, A. R. Calawa, Z. Liliental-Weber, submitted to J. Appl. Phys., 12/95.
18. M. A. Lampert and P. Mark (eds), *Current injection in solids*, (New York, Academic Press, 1970).
19. S. A. McQuaid, R.C. Newman, M. Missous and S. Ohagan, Appl. Phys. Lett. **61**, 3008 (1992).
20. J. Dabrowski and J. E. Northrup, Phys. Rev. B **49**, 14286 (1994).
21. F. H. Baumann, J.-H. Huang, J. A. Rentschler, T. Y. Chang, A. Ourmazd, Phys. Rev.Lett. **73**, 448 (1994).
22. C. Kisielowski, P. Schwander, Y. Kim, J.-L. Rouviere, A. Ourmazd, Phys. Stat. Sol. (a) **137**, 557 (1993).
23. see e.g. U. Goesele, T. Y. Tan in *Materials Science and Technology 4*, W.Schroeter (ed.), VCH Verlagsgemeinschaft, Wernheim/Germany, 1991.
24. M. Gribeljuk, C. Kisielowski, F. H. Baumann, A. Ourmazed, unpublished.
25. J. C. H. Spence, J. M. Zuo, *Electron Microdiffraction*, (Plenum Press, New York, 1992).
26. see e.g. *Microscopy and Microanalysis* 1995, G. W. Bailey, M. H. Ellisman, R. A. Henningar, N. J. Zaluzec (eds.), Jones & Begell Publishing, New York, 1995.
27. Z. Liliental-Weber, C. Kisielowski, Y. Chen, J. Washburn, I. Grzegory, M. Bockowski, J.Jun, S. Porowski, submitted to J. Appl. Phys.12/95.
28. P. Boguslawski, E. L. Briggs, J. Bernholc, Phys. Rev. B**51**, 17255 (1995).